Inhibition of striatal cholinergic interneuron activity by the Kv7 opener retigabine and the nonsteroidal anti-inflammatory drug diclofenac

Rodrigo Manuel Paz [a, 1], Cecilia Tubert [a, 1, 3], Agostina Stahl [a], Analía López Díaz [a], Roberto Etchenique [b], Mario Gustavo Murer [a, 2], Lorena Rela [a, *, 2]

[a] Universidad de Buenos Aires y Consejo Nacional de Investigaciones Científicas y Técnicas (CONICET), Instituto de Fisiología y Biofísica "Bernardo Houssay" (IFIBIO-Houssay), Grupo de Neurociencia de Sistemas, Buenos Aires 1121, Argentina
[b] Departamento de Química Inorgánica, Analítica y Química Física, INQUIMAE, Facultad de Ciencias Exactas y Naturales, Universidad de Buenos Aires, CONICET, Ciudad Universitaria Pabellón 2, AR1428EHA Buenos Aires, Argentina

ARTICLE INFO

ABSTRACT

Striatal cholinergic interneurons provide modulation to striatal circuits involved in voluntary motor control and goal-directed behaviors through their autonomous tonic discharge and their firing "pause" responses to novel and rewarding environmental events. Striatal cholinergic interneuron hyperactivity was linked to the motor deficits associated with Parkinson's disease and the adverse effects of chronic antiparkinsonian therapy like L-DOPA-induced dyskinesia. Here we addressed whether Kv7 channels, which provide negative feedback to excitation in other neuron types, are involved in the control of striatal cholinergic interneuron tonic activity and response to excitatory inputs. We found that autonomous firing of striatal cholinergic interneurons is not regulated by Kv7 channels. In contrast, Kv7 channels limit the summation of excitatory postsynaptic potentials in cholinergic interneurons through a postsynaptic mechanism. Striatal cholinergic interneurons have a high reserve of Kv7 channels, as their opening using pharmacological tools completely silenced the tonic firing and markedly reduced their intrinsic excitability. A strong inhibition of striatal cholinergic interneurons was also observed in response to the anti-inflammatory drugs diclofenac and meclofenamic acid, however, this effect was independent of Kv7 channels. These data bring attention to new potential molecular targets and pharmacological tools to control striatal cholinergic interneuron activity in pathological conditions where they are believed to be hyperactive, including Parkinson's disease.

© 2018 Elsevier Ltd. All rights reserved.

1. Introduction

The striatal cholinergic interneurons (SCIN) are regarded as key modulators of voluntary movement and goal directed behavior. Selective ablation and optogenetic studies involve SCIN in motor control, instrumental learning, behavioral flexibility, motivation and social behavior (Witten et al., 2010; Aliane et al., 2011; Bradfield et al., 2013; Maurice et al., 2015; Martos et al., 2017). Recent studies support long standing theories involving SCIN in Parkinson's disease symptoms (Maurice et al., 2015; Kharkwal et al., 2016; Aldrin-Kirk et al., 2018) and also in L-DOPA-induced dyskinesia (Won et al., 2014; Bordia et al., 2016), a common adverse effect of antiparkinsonian therapy. While modulating SCIN influence over the striatal circuit may have therapeutic significance, this is not achieved through the systemic administration of "anticholinergic" drugs because of their multiple targets and effects (Kalia and Lang, 2015). A better knowledge of SCIN physiology may provide better targets for therapeutic interventions in Parkinson's disease and other movement disorders.

SCIN are capable of generating patterns of action potential discharge in the absence of synaptic input (Bennett and Wilson, 1999; Cragg, 2006; Pisani et al., 2007). Calcium-dependent

---

potassium currents (KCa) and the hyperpolarization-activated depolarizing current Ih interact to push the membrane potential periodically to the action potential threshold (Goldberg and Wilson, 2005; Deng et al., 2007). Synaptic inputs transiently change this pattern, inducing signals that encode salient environmental events (Ding et al., 2010). SCIN also have voltage-dependent potassium currents (Kv) whose roles in SCIN physiology are poorly understood (Song et al., 1998). During studies aimed at disclosing the role of Kv currents in SCIN spike frequency adaptation (a slowing of discharge rate occurring during sustained depolarization that may be followed by a complete stop of firing due to spike threshold accommodation), we found that the prototypic Kv7 blocker XE991 has no effect on SCIN excitability (Sanchez et al., 2011; Tubert et al., 2016). This was surprising given the expression of Kv7.2 subunits in SCIN (Cooper et al., 2001) and the well-known role of Kv7 channels in neuronal excitability (Brown et al., 2009).

Kv7 channels display subthreshold activation, do not inactivate and mediate the M-current, which has marked effects on excitability (Wang et al., 1998; Brown and Passmore, 2009). They have been involved in stabilization of neuronal resting membrane potential, regulation of action potential generation and propagation, burst firing, and intrinsic long-term plasticity (Yue and Yaari, 2006; Wu et al., 2008; Battefeld et al., 2014). Additionally, Kv7 channels limit the release probability in the calyx of Held (Huang and Trussell, 2011) and EPSP temporal summation in hippocampal, cortical pyramidal and striatal medium spiny neurons (Hu et al., 2002; Shen et al., 2005; Lee and Kwag, 2012). Kv7 function in a given neuron depends on the subunit composition and/or subcellular localization of the channels (Brown and Passmore, 2009; Cooper, 2011) and their regulation by different neurotransmitter receptors and signaling pathways (Brown, 2017).

There are five Kv7 subunits that can form homo or heterotetramers with different functional and pharmacological properties. Four of them (Kv7.2-Kv7.5) are expressed in the brain (Jentsch, 2000). Recent studies revealed subtype-specific effects of several drugs on Kv7 channels (Soh and Tzingounis, 2010; Brueggemann et al., 2011). Interestingly, the cyclooxygenase (COX) inhibitor diclofenac, a nonsteroidal anti-inflammatory drug (NSAID), may behave as an opener or blocker of Kv7 channels depending on their subunit composition (Brueggemann et al., 2011). Here we studied the expression of Kv7 subunits in SCIN and the effect on them of several Kv7 channel openers and blockers to further understand the role of Kv7 channels in SCIN physiology.

2. Materials and methods

Subjects. Mice allowing the identification of SCIN through cell type-specific expression of the fluorescent protein tdTomato (ChAT-Cre; tdT, for simplicity) were obtained by crossing ChAT-Cre [B6; 129S6-Chat$^{tm2(cre)Lowl}$/J, Stock 6410, The Jackson Laboratories (Rossi et al., 2011)] and Rosa-CAG-LSL-tdTomato-WPRE mice [B6.Cg-Gt(ROSA)26Sor$^{tm14(CAG-tdTomato)Hze}$/J, stock 7914, The Jackson Laboratories (Madisen et al., 2010)]. Mice were 15–45 days old. Up to six mice were housed per cage with water and food *ad libitum* and 12:12 h light/dark cycle (lights on at 7:00 a.m.) and cared for in accordance with institutional guidelines (IACUC of the School of Medicine, University of Buenos Aires, 2598/13).

Acute slicing. Male mice were anesthetized with isoflurane and decapitated. The brain was quickly removed, chilled in ice-cold low Ca^{2+}-high Mg^{2+} ACSF and prepared for slicing. Three hundred-μm-thick coronal slices at the level of the striatum were cut using a vibratome (Pelco T series 1000, Ted Pella). Slices were submerged in low Ca^{2+}-high Mg^{2+} ACSF at 34 °C for 30 min and then kept in this ACSF at room temperature in a recovery chamber. ACSF composition was as follows (in mM): 125 NaCl, 2.5 KCl, 1.3 NaH$_2$PO$_4$·H$_2$O, 26 NaHCO$_3$, 2 CaCl$_2$, 1 MgCl$_2$, and 10 glucose. For low Ca^{2+}-high Mg^{2+} ACSF, 0.5 mM CaCl$_2$ and 2.5 mM MgCl$_2$ were used.

Electrophysiological recordings. Slices were transferred to a submersion type chamber perfused by a peristaltic pump (Ismatec, Germany) with ACSF at a constant rate of 3 ml/min; temperature in the recording chamber was set at 34 °C with a TC-344B temperature controller (Warner Instruments). Cells were visualized using an upright microscope (Nikon Eclipse) equipped with a 40× water-immersion objective, DIC and fluorescence optics, and an infrared camera connected to a monitor and computer. Recording electrodes were made with borosilicate glass capillaries shaped with a puller (P-97, Sutter Instruments). For whole-cell recordings, electrodes were filled with internal solution containing the following (in mM): 20 KCl, 120 K-gluconate, 10 HEPES, 3 Na$_2$ATP, 0.3 NaGTP, 0.1 EGTA, 10 phosphocreatine and 2 MgCl$_2$, pH 7.3 adjusted with KOH. For cell-attached recordings the pipettes were filled with ACSF. Recordings were amplified (Axopatch-1D; Molecular Devices), sampled at 20 kHz (Digidata 1322A, Molecular Devices) and acquired on a PC running pClamp 9.2 (Molecular Devices). Cells considered for data analysis fulfilled the following criteria for whole-cell recordings: series resistance between 10 and 30 MΩ, action potential amplitude ≥50 mV from threshold to peak and resting membrane potential between −75 and −45 mV. Synaptic responses were evoked by intrastriatal electric stimulation with a bipolar electrode placed at ~500 μM from the recorded cell (20 Hz, 0.1 ms pulse duration). Glutamate uncaging was elicited by light pulses (20 Hz, 0.1 ms pulse duration) generated with a 447 nm, 1 W LED and delivered through an optic fiber (Tolket, Argentina) placed <300 μm from the recorded cell (5 mW measured at the optic fiber tip).

Pharmacological manipulations. Unless otherwise stated, reagents were purchased from Sigma (Argentina). Salts were purchased from Baker (Chemical Center, Argentina). Drugs were prepared as stock solutions, diluted in ACSF immediately before use and applied through the perfusion system. The following stock solvents and final concentrations were used: distilled H$_2$O for diclofenac (30, 100 and 300 μM) and MFA (100 μM); DMSO for CNQX (40 μM), XE991 (30 μM), picrotoxin (100 μM), linopirdine (10 μM, Alomone Labs), and retigabine (10 μM, Alomone Labs); ethanol for UCL2077 (10 μM, Tocris); ACSF for RubiGlutamate (300 μM). RubiGlutamate was synthesized as reported in Fino et al. (2009) and is commercially available from Tocris (Cat# 3574).

Acquisition and analysis of electrophysiological data. Data acquisition and analysis were performed with ClampFit (Molecular Devices). Resting membrane potential was measured at the baseline before the injection of current pulses and the input resistance was calculated as the slope of the V/I curve with V measured at the steady-state of the response to 1-sec, −10 to +50 pA current pulses. Sag amplitude was measured as the difference between the peak hyperpolarization and the steady-state of the response elicited by a 1-s, −40 pA current pulse. Slow afterhyperpolarization (sAHP) amplitude was measured as the difference between the peak hyperpolarization elicited after the end of the current pulse of +140 pA and the membrane potential just before the current step (baseline). Rheobase was calculated as the minimal amplitude of a 1-s current step that resulted in the firing of at least one spike. Action potential threshold was obtained from action potential phase plots as the point at which the derivative of the membrane potential dV/dt deviated from the mean baseline value by > 5 standard deviations (Atherton and Bevan, 2005). The width of the action potential was calculated at 50% of the maximal amplitude, measured from threshold to peak. Threshold, width and amplitude were measured only for the first spike elicited at rheobase. Average firing frequency in the cell-attached configuration was determined during 5 min of recording after 8 min of perfusion with the specified solutions.

Immunohistochemistry. Immunostaining was performed in paraformaldehyde-fixed free-floating sections as previously reported (Braz et al., 2015; Tubert et al., 2016). ChAT-Cre;tdT mice were anesthetized with chloral hydrate (600 mg/kg, i.p.), perfused through the ascending aorta with 0.1 M phosphate buffered saline, pH 7.4 (PBS) supplemented with heparin (2U/ml, Rivero, Argentina) followed by 4% paraformaldehyde in PBS. Brains were removed, post-fixed for 4 h in the same fixative, cryoprotected in 30% sucrose/PBS and cut at 40 μm with a sliding-freezing microtome (Leica). Sections containing the striatum were preserved in PBS with 0.1% sodium azide. Sections were blocked for 30 min at room temperature with 2% bovine serum albumin (BSA) and 0.3% Triton X-100 in PBS (blocking buffer), incubated overnight with primary antibodies [Rabbit anti-Kv7.2, Kv7.3, Kv7.4 and Kv7.5, APC-050 (RRID: AB_2040101), APC-051 (RRID: AB_2040103), APC-164 (RRID: AB_2341042) and APC-155 (RRID: AB_2341038), Alomone Labs, all at 1:100 dilution] at 4 °C in the same buffer, washed 3 times in PBS with 0.3% Triton X-100 (PBST) and incubated in blocking buffer with secondary antibodies conjugated to Alexa Fluor 488 (A11034, Invitrogen, 1:1000) at room temperature for 2 h. Sections were then washed in PBST followed by PBS, mounted on glass slides with Vectashield (Vector) and coverslipped.

Image acquisition and analysis. Images were acquired with an Olympus FV1000/IX81 confocal microscope as single sections, using an oil-immersion objective (40×; numerical aperture, 1.3). Digital images were color balanced with Adobe Photoshop 8.0 (Adobe Systems). The composition of the images was not altered. To quantify the percentage of SCIN positive for Kv7 subunits in confocal images of immunostained striatal tissue sections SCIN somata were detected by an automated method applied to the tdTomato channel (Otsu thresholding and particle analysis, Image J) (Schneider et al., 2012) and the average intensity of the Kv7 label was quantified in the detected particles. Cells were considered positive for Kv7 subunits when the average intensity value was >2 SD above the average fluorescence intensity of an adjacent region of neuropil of comparable size. A total of 163 SCIN somata from 5 mice were analyzed for colocalization with Kv7 subunits.

Laser capture microdissection. Mice were anesthetized and perfused with PBS as described above followed by 2% paraformaldehyde/PBS and subsequently by 20% sucrose/PBS. Brains were removed, rapidly frozen in Cryoplast embedding medium (Biopack, Argentina), sectioned at 10 μm using an RNase-free cryostat (Thermo Cryotome E) and mounted in positively charged microscope slides. Laser capture microdissection was performed according to Rossi et al., 2012. Briefly, the infrared (IR)-laser energy of an Arcturus laser capture microdissection equipment (Applied Biosystems) combined with the ultraviolet (UV) cutting laser were used for circumscription of tdTomato-positive neurons. Then, a High Sensitive (HS) CapSure laser capture microdissection cap (Applied Biosystems) containing a thermoplastic film was placed over the target area. By pulsing the IR-laser through the cap, the thermoplastic film forms a thin protrusion that bridges the gap between the cap and tissue and adheres to the target neuron. By lifting the cap, target neurons now attached to the cap were removed. Approximately 200 neurons were captured on each cap. As negative control, striatal tissue without tdTomato-positive somata was captured.

RNA isolation and RT-PCR. Total RNA was extracted from samples obtained by laser capture microdissection using the Paradise PLUS Reagent system (Applied Biosystems) following the manufacturer's instructions. To improve RNA yield, samples were digested for 16 h at 37 °C in the presence of 20 μg Proteinase K (Applied Biosystems). Samples were incubated with RNase-free DNAse (1 unit per μg RNA, Promega Corporation) at room temperature for 20 min to degrade contaminating DNA. Oligo(dT)-primed cDNA was
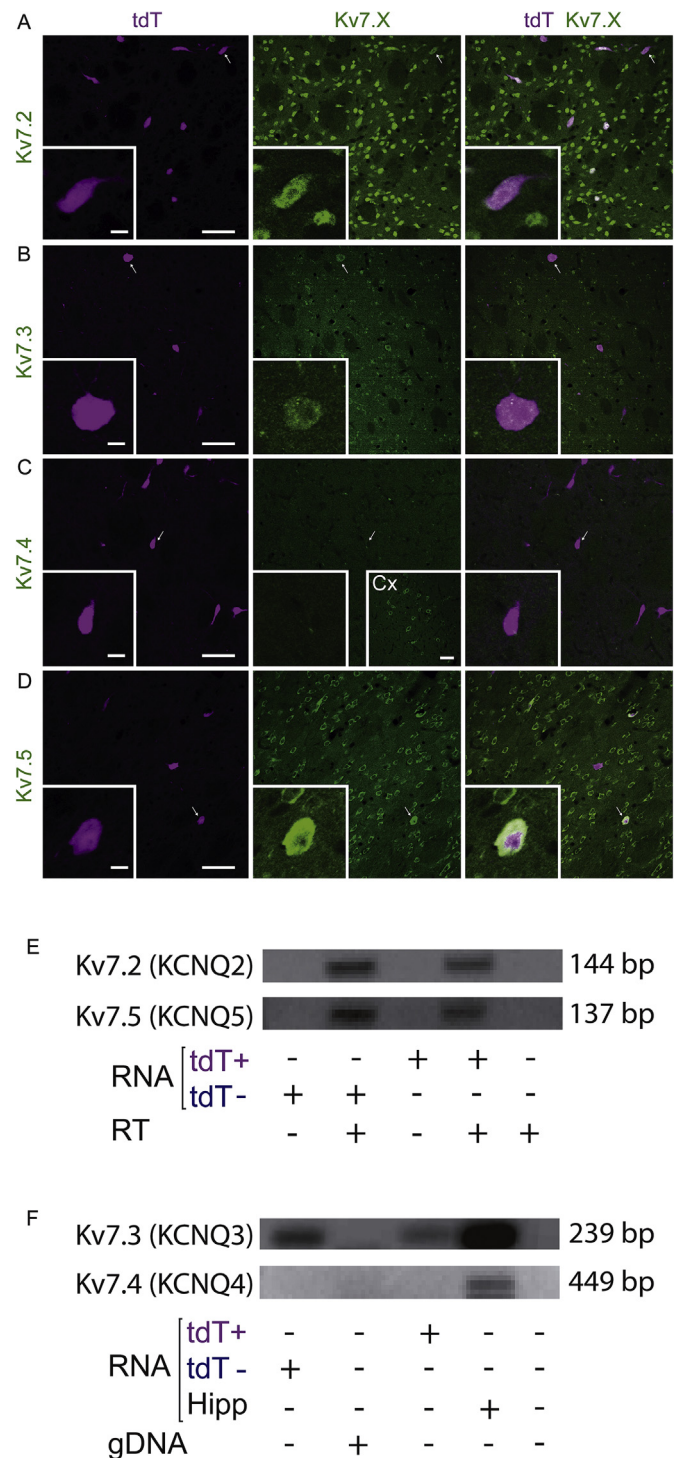
Fig. 1. SCIN express Kv7.2, Kv7.3 and Kv7.5 subunits. A-D. Dorsolateral striatal region of a representative ChAT-Cre;tdT mouse immunolabeled with antibodies directed against Kv7 subunits showing colocalization of tdTomato (tdT, magenta) with Kv7.2 (A), Kv7.3 (B) and Kv7.5 (D) (green), and no expression of Kv7.4 (C). Bars: 50 μm. Insets at the left show magnified SCIN somata indicated by the arrows; inset at the right in C show a positive control with Kv7.4 expression in cortex (Cx); inset bars: cortex 50 μm; striatum 10 μM. **E and F.** The mRNA expression of Kv7.2, Kv7.5 (**E**) Kv7.3 and Kv7.4 (**F**) in tdTomato positive (tdT+) and negative (tdT-) striatal samples analyzed by RT-PCR is shown. For negative controls the product of a retrotranscription reaction without RNA or retrotranscriptase (E) or amplification with genomic DNA as template (F) were used. For positive control, hippocampal cDNA was used.
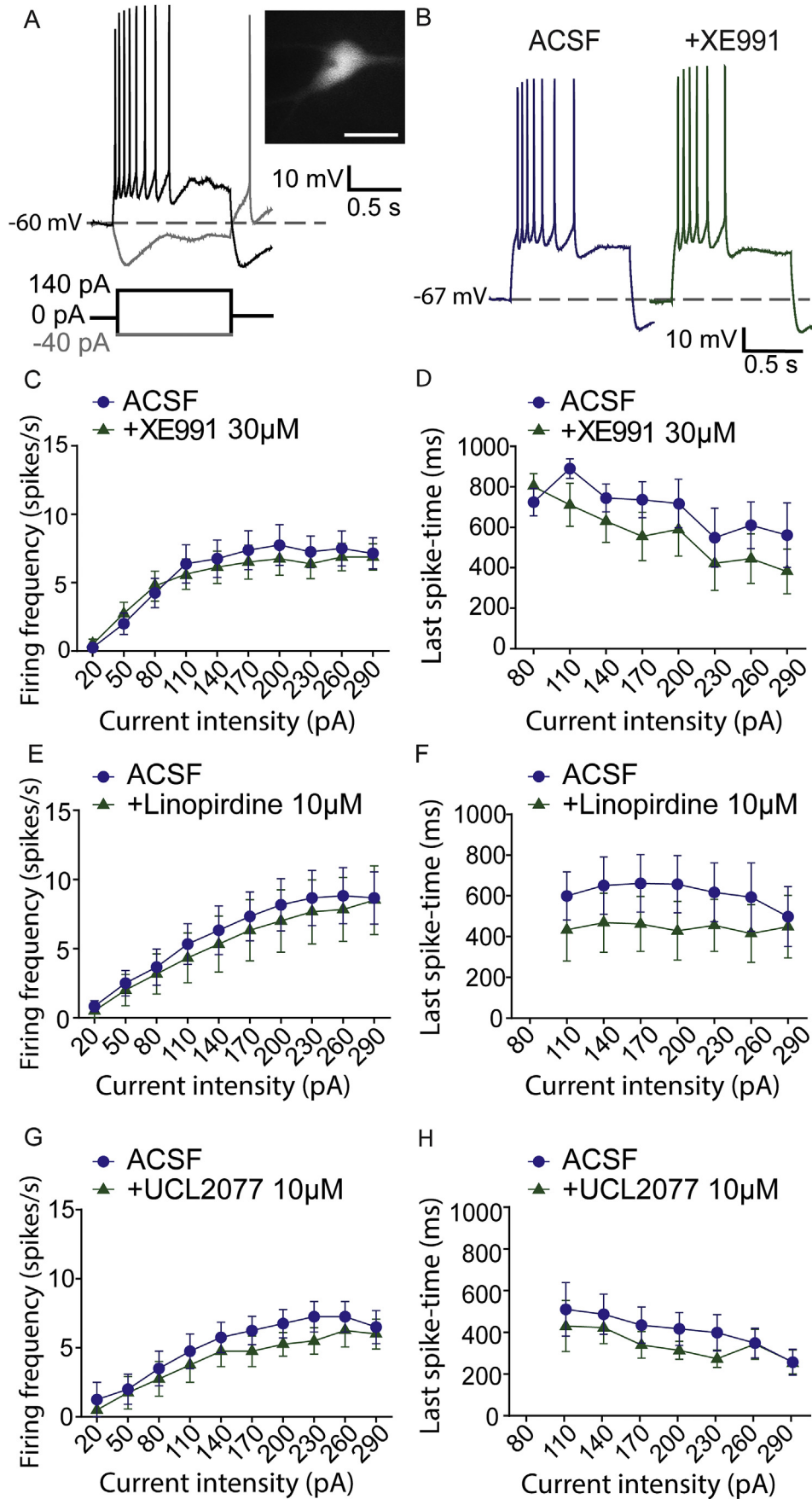
synthesized from total RNA obtained from each laser capture sample using the ImProm-II Reverse Transcription System (Promega), adjusting the $MgCl_2$ concentration to 4.75 mM. Negative controls consisted of RNA or reverse transcriptase omission in the RT reaction, or genomic DNA use as template in subsequent PCR analysis. cDNA was amplified with the selected primers (Kv7.2: 5′-ACTGCCTGGTACATTGGCTT-3′, 5′-CCCCGTAGCCAATGGTCGTC-3′; Kv7.3: 5′-CACCGTCAGAAGCACTTTGAG-3′, 5′-CCTTTAGTATTGCTAC-CACGAGG-3′; Kv7.4: 5′-GCTTACGGTGGATGATGTCA-3′, 5′-TGTGGTAGTCCGAGGTGATG-3′; Kv7.5: 5′-GTCGGCGCAACGT-CAAGTA-3′, 5′-AACCAAACACAAGGAGAAAAACG-3′) in 35 rounds of conventional PCR amplification using a PTC-100 thermal cycler (MJ Research) and the GoTaq DNA Polymerase following manufacturer's instructions with minor changes (Taq Polymerase was used at 2U per reaction and primers at 1.1 μM). Each cycle included denaturation at 94 °C for 30 s, annealing for 1 min (50 °C for Kv7.2-4 and 52 °C for Kv7.5) and extension at 72 °C for 1 min. PCR products were subjected to electrophoresis through a 2% agarose gel with 0.5 μg/ml ethidium bromide for product visualization under UV illumination. A 100 pb ladder (Embiotec, Argentina) was used to confirm product molecular weights. Independent samples from three animals were analyzed for Kv7.2 and Kv7.5 and from two animals for Kv7.3 and Kv7.4, yielding comparable results.

Statistical analyses. Statistical analysis details can be found in the figure legends and wherever numerical data is presented in the text. Paired t-tests were used to compare two samples and two-way ANOVA with repeated measures was used to analyze the effects of drug treatments on responses to different intensities of stimulation or at different time points. Data were tested for normality and homoscedasticity (SigmaPlot 11.0). Non-parametric tests were used when these criteria were not met (Wilcoxon to compare two paired samples). Significance level was set at *p<0.05*, and all data are expressed as mean ± SEM unless otherwise specified. GraphPad Prism version 6.00 for Windows (GraphPad Software) and Matlab routines were used for data analysis. Sidak corrections were applied for multiple comparisons.

3. Results

3.1. SCIN express several Kv7 subunits

Kv7 channels modulate spike frequency adaptation, spike threshold accommodation and the slow afterhyperpolarization (sAHP) in neurons of the hippocampus and other structures (Brown and Passmore, 2009). These are prominent features of SCIN (Jiang and North, 1991; Bennett and Wilson, 1999; Maurice et al., 2004) and SCIN express Kv7.2 (Cooper et al., 2001), however, we previously found that the prototypic Kv7 channel blocker XE991 (10 μM) has no effect on SCIN excitability (Sanchez et al., 2011; Tubert et al., 2016).

To confirm the presence of Kv7 channels, we studied the expression of Kv7 subunits in SCIN by means of immunohistochemistry in coronal brain sections of ChAT-Cre;tdT mice which allow the visualization of cholinergic neurons through the endogenous expression of tdTomato (Tubert et al., 2016). Subunits 7.2 and

7.5 were expressed in 97.8 ± 2.2% and 98.0 ± 2.0% of SCIN respectively, while Kv7.3 was expressed by 39.8 ± 11.1% of SCIN and Kv7.4 was not detected (Fig. 1A–D). None of the subunits was exclusively expressed in SCIN; additional striatal elements were labeled by the antibodies, except for the anti-Kv7.4 antibody, which did not label striatal cells but labeled cells in the cortex (Fig. 1C). To assess further Kv7 subunit expression in SCIN we obtained tissue samples containing or excluding SCIN from ChAT-Cre;tdT mice striatal sections by laser capture microdissection. We have previously demonstrated that these SCIN samples are enriched in ChAT mRNA (Tubert et al., 2016). Consistently with the above described immunohistochemical findings, the mRNAs of Kv7.2, 7.3 and 7.5 were detected in SCIN samples and non-SCIN samples (Fig. 1E–F), whereas Kv7.4 mRNA was not detected in the striatum (Fig. 1F). Overall, the data show that SCIN express several Kv7 channel subunits.

3.2. Lack of effect of Kv7 blockers on SCIN somatic excitability

To address a putative effect of Kv7 channels on SCIN excitability, we tested a higher dose of XE991 (30 μM) than the one previously used (Sanchez et al., 2011; Tubert et al., 2016) (Fig. 2A–D) and the effects of two additional Kv7 blockers, linopirdine and UCL2077, on the response of SCIN to current injection (Fig. 2E–H). The Kv7 channel blockers had no effect on SCIN excitability and accommodation as shown by unaltered firing frequency (Fig. 2C, E, G) and last spike time (Fig. 2D, F, H) of responses to current steps. Moreover, XE991 (30 μM) increased input resistance (135.1 ± 12.4 MΩ before and 190.4 ± 16.7 MΩ after adding XE991; p = 0.0097, slope comparison in linear regression of V/I curve) and had a small effect on action potential threshold without changing other physiological properties of SCIN, including resting membrane potential, sag and sAHP amplitude, rheobase and action potential amplitude and duration (Table 1). Overall the data confirm and extend previous findings by showing little effects of Kv7 channel blockers on the somatic response of SCIN to current injection.

3.3. Kv7 blockers reduce synaptic integration in SCIN without affecting spontaneous pacemaking

To determine if Kv7 channels are recruited by physiologically relevant patterns of SCIN activity, we studied the effect of Kv7 channel blockers on SCIN spontaneous pacemaking (Fig. 3) and SCIN responses to glutamatergic input (Figs. 4–6).

Spontaneous spike discharges were recorded in the cell-attached configuration with picrotoxin and CNQX in the bath to minimize regulation by extrinsic signals (Fig. 3A). XE991 failed to modify spontaneous SCIN discharge (Fig. 3B–C).

Kv7 channels modulate subthreshold EPSP summation in neurons of the hippocampus and other structures (Hu et al., 2002; Shen et al., 2005; Lee and Kwag, 2012). This is often connected to their effects on action potential discharge but a dissociation between Kv7 effects on EPSP summation and axon potential initiation has also been reported (Hönigsperger et al., 2015). To determine if Kv7 channels modulate EPSP summation in SCIN we electrically

Fig. 2. Kv7 blockers have no effect on SCIN somatic excitability. A. Representative whole cell response of a SCIN to depolarizing and hyperpolarizing current steps. Inset: endogenous fluorescence of a SCIN in a striatal slice of a ChAT-Cre;tdT mouse. Bar: 50 μM. **B.** Representative response of a SCIN to a depolarizing 1 s 140 pA current step before (blue) and after (green) bath application of XE991 (30 μM). CNQX and picrotoxin in the bath prevented indirect effects via AMPA and GABA-A receptors. **C and D.** Firing frequency (C) and last spike time (D) versus current intensity before and after XE991 (30 μM). **E and F.** Firing frequency (E) and last spike time (F) versus current intensity before and after linopirdine (10 μM). **G and H.** Firing frequency (G) and last spike time (H) versus current intensity before and after UCL2077 (10 μM). Data are mean ± SEM. Statistical analysis: two-way repeated measures (RM) ANOVA with drug treatment and current intensity as factors [**C:** $F_{interaction}(9, 63) = 1.588$, p = 0.1383, $F_{treatment}(1, 7) = 0.5965$, p = 0.4652, n = 8 from 5 mice; **D:** $F_{interaction}(7, 35) = 1.115$, p = 0.3756, $F_{treatment}(1, 5) = 4.448$, p = 0.0887, n = 6 from 4 mice; **E:** $F_{interaction}(9, 45) = 0.5858$, p = 0.8016, $F_{treatment}(1, 5) = 0.4708$, p = 0.5231, n = 6 from 2 mice; **F:** $F_{interaction}(6, 24) = 1.191$, p = 0.3442, $F_{treatment}(1, 4) = 1.617$, p = 0.2724, n = 5 from 2 mice; **G:** $F_{interaction}(9, 27) = 1.667$, p = 0.1465, $F_{treatment}(1, 3) = 6.122$, p = 0.0897, n = 4 from 2 mice; **H:** $F_{interaction}(6, 18) = 1.954$, p = 0.1265, $F_{treatment}(1, 3) = 3.910$, p = 0.1424, n = 4 from 2 mice]. For D, F and H data from low intensity pulses were excluded to keep at least 4 cells with spikes at all intensities. (For interpretation of the references to color in this figure legend, the reader is referred to the Web version of this article.)

Table 1
Comparison of SCIN electrophysiological features before and after XE991. The recordings were performed in the presence of 100 μM picrotoxin and 40 μM CNQX. XE991 was used at 30 μM. The values represent the mean ± SEM (n = 8). Statistical test: Wilcoxon, except for input resistance which used a slope comparison in linear regression analysis from graphpad software.

Property	ACSF	XE991	p value
Resting membrane potential (mV)	−65.3 ± 1.04	−64.5 ± 1.23	0.2500
Input resistance (MΩ)	135.1 ± 12.4	190.4 ± 16.7	**0.0097**
Sag amplitude (mV)	3.2 ± 0.79	3.18 ± 0.86	0.9844
Sag latency (ms)	141.5 ± 41.72	140.1 ± 28.32	0.3828
sAHP amplitude (mV)	6.5 ± 1.53	6.06 ± 1.29	0.9375
Rheobase (pA)	68.8 ± 16.95	57.5 ± 10.98	0.7500
Threshold (mV)	−41.7 ± 0.88	−40.7 ± 1.00	**0.0078**
Amplitude of 1st spike (mV)	74.7 ± 2.85	72.7 ± 2.65	0.3125
Width of 1st spike (ms)	1.4 ± 0.06	1.6 ± 0.14	0.0781

stimulated striatal afferents (5 pulses at 20 Hz) in the presence of picrotoxin in the bath (Fig. 4A). Addition of XE991 (10 μM or 30 μM) significantly increased the amplitude of the first EPSP [1.3 ± 0.1 mV before and 1.5 ± 0.2 mV after adding 10 μM XE991, paired *t*-test, t(5) = 3.679, p = 0.0143; 1.8 ± 0.3 mV before and 2.5 ± 0.2 mV after adding 30 μM XE991, paired *t*-test, t(3) = 6.223, p = 0.0084] and EPSP summation in these conditions (Fig. 4B–C), without affecting the resting membrane potential [−66.3 ± 0.5 mV before and −66.0 ± 0.5 mV after adding 10 μM XE991, paired *t*-test, t(5) = 1.682, p = 0.1534; −65.3 ± 1.7 mV before and −64.9 ± 1.7 mV after adding 30 μM XE991, paired *t*-test, t(3) = 0.4319, p = 0.6950]. Similarly, addition of linopirdine (10 μM) to the bath in a separate SCIN sample also enhanced EPSP summation (Fig. 5A–C), without changing the resting membrane potential [−66.5 ± 1.0 mV before and −66.6 ± 0.9 mV after adding linopirdine, paired *t*-test, t(5) = 0.0622, p = 0.9528]. The increase in amplitude of the first EPSP after linopirdine did not reach statistical significance [1.1 ± 0.2 mV before and 1.9 ± 0.5 mV after adding linopirdine, paired *t*-test, t(5) = 2.354, p = 0.0652].

Because Kv7 channels can regulate neurotransmitter release (Huang and Trussell, 2011) and presynaptic versus postsynaptic effects of Kv7 blockers cannot be distinguished in the above experiments, we studied the effect of XE991 on SCIN responses evoked by glutamate uncaged from RuBi-glutamate in the presence of picrotoxin in the bath (Fino et al., 2009). RuBi-glutamate was added to the bath and excited with trains of blue light pulses (0.1 ms, 5 pulses at 20 Hz) delivered through the tip of an optic fiber located near the recorded SCIN (Fig. 6A). Responses evoked by light trains resembled those evoked by trains of electrical stimuli and were blocked by glutamate receptor antagonists (Fig. 6B). Addition

of XE991 (30 μM) significantly increased the amplitude of the first EPSP [0.96 ± 0.1 mV before and 1.2 ± 0.1 mV after adding XE991, paired *t*-test, t(5) = 2.843, p = 0.0361] and EPSP summation (Fig. 6C), without affecting the resting membrane potential [-65.3 ± 1.5 mV before and −66.5 ± 1.4 mV after adding XE991, paired *t*-test, t(5) = 0.8116, p = 0.4539].

Similar to depolarizing somatic current injections, EPSP trains are followed by an sAHP in SCIN, which has been compared with the pause response shown by SCIN in response to salient environmental events (Reynolds et al., 2004; Tubert et al., 2016). This sAHP could be mediated by depolarization-activated potassium currents (Reynolds et al., 2004; Wilson, 2005). However, the amplitude of the sAHP that follows EPSPs evoked by electrical stimulation was not changed by XE991 (Fig. 4D) or linopirdine (Fig. 5D), while the sAHP that follows glutamate evoked EPSPs was enhanced after adding XE991 to the bath (Fig. 6D).

Overall, the data show that SCIN Kv7 channels provide negative feedback during EPSP summation without affecting spontaneous tonic discharge. Additionally, they suggest that the sAHP that follows an EPSP train is mediated by other currents, consistently with previous studies (Sanchez et al., 2011; Tubert et al., 2016).

3.4. The Kv7 opener retigabine reduces SCIN excitability and spontaneous tonic discharge

The above findings suggested that SCIN Kv7 channels are involved only in particular physiological conditions like during dendritic integration of EPSPs. To determine if Kv7 channels can be recruited to modulate SCIN action potential firing and spontaneous activity, we exposed SCIN to the Kv7 channel opener retigabine. Retigabine produces a hyperpolarizing shift of the activation curve of Kv7 channels (Main et al., 2000; Wickenden et al., 2000; Tatulian et al., 2001). Thus, we tested if retigabine modulates SCIN excitability and autonomous pacemaking by recruiting Kv7 channels.

Retigabine in the bath (10 μM) markedly decreased SCIN excitability and accommodation as shown by a decreased firing frequency and a shorter last spike time during responses to 1-s depolarizing current steps, and XE991 (30 μM) completely blocked its effects (Fig. 7A–C). Furthermore, the tonic discharge observed in SCIN in the presence of CNQX and picrotoxin was significantly reduced by retigabine and partially restored by addition of XE991 (Fig. 7D–E). These effects of retigabine were associated to a significant increase of the rheobase current and a significant 2.5 mV more depolarized action potential threshold, without changes in resting membrane potential, input resistance and action potential amplitude, duration and latency (Table 2). Overall, the data show
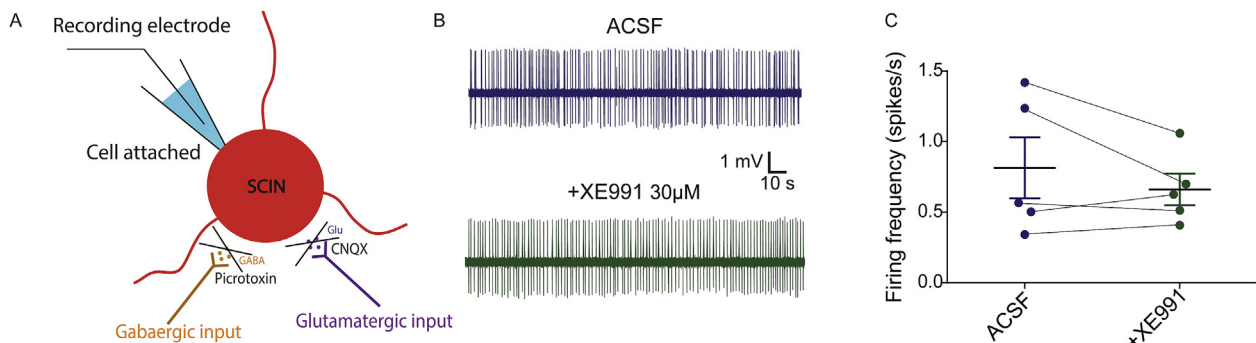
Fig. 3. Kv7 blockers do not affect SCIN spontaneous activity. A. Schematic diagram of a cell attached recording of spikes generated by a SCIN. CNQX and picrotoxin in the bath prevented indirect effects via AMPA and GABA-A receptors. **B and C.** Representative recordings of a SCIN (B) in the absence (blue) or presence (green) of XE991 and average spontaneous firing frequency (C) [Paired *t*-test, t(4) = 1.193, p = 0.2987, n = 5 SCIN from 3 mice]. Data are mean ± SEM. (For interpretation of the references to color in this figure legend, the reader is referred to the Web version of this article.)
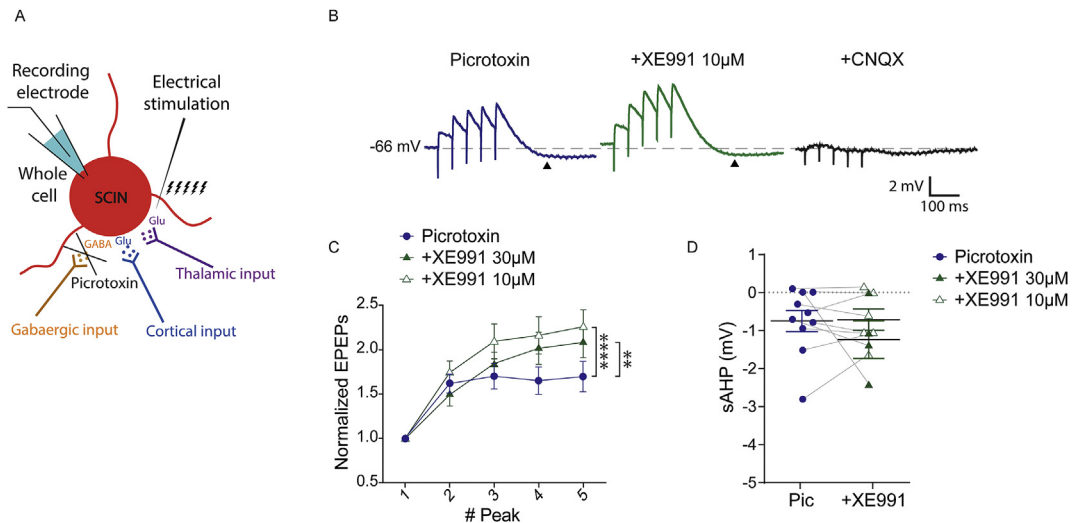
Fig. 4. XE991 enhances synaptic temporal integration of SCIN responses to electrical stimulation. A. Schematic diagram of whole cell recordings of EPSPs induced by locally stimulating striatal afferents. **B.** Representative responses of a SCIN to afferent stimulation (5 pulses at 20 Hz) before (blue) and after (green) adding XE991 (10 μM) to the bath. Addition of CNQX (40 μM) blocked the response to stimulation. **C.** Average normalized EPSP amplitude in control conditions and in the presence of XE991. Absolute amplitudes are shown in Fig. S2B. **D.** Average amplitude of the sAHP measured at the point indicated by the arrowhead in B. Statistical analysis: two-way RM-ANOVA with drug treatment and EPSP number as factors [**p = 0.0098, $F_{interaction}(4,12) = 5.441$, n = 4; ****p < 0.0001, $F_{interaction}(4,20) = 12.85$, n = 6]. (For interpretation of the references to color in this figure legend, the reader is referred to the Web version of this article.)

that Kv7 channels are potentially capable of modulating SCIN somatic excitability and spontaneous activity.

3.5. The nonsteroidal anti-inflammatory drugs diclofenac and meclofenamic acid inhibit SCIN through an XE991-insensitive mechanism

Some Kv7 modulators like the NSAID diclofenac behave as openers or blockers of Kv7 channels depending on their subunit composition. For instance, diclofenac behaves as an opener when channels are composed of Kv7.2, Kv7.3 and Kv7.4 subunits but it blocks Kv7.5 channels (Peretz et al., 2005; Brueggemann et al., 2011). To address the composition of SCIN Kv7 channels, we tested the effect of diclofenac on SCIN excitability. Addition of diclofenac to the bath powerfully and dose dependently decreased SCIN excitability, but its effect was not blocked by XE991 (Fig. 8A–D). Moreover, diclofenac inhibited SCIN tonic discharge, and again, its effect was not reversed by XE991 (Fig. 8E–F).

We then asked whether meclofenamic acid (MFA), which produces a leftward shift in the activation curve of Kv7 channels comparable to the one produced by diclofenac (Peretz et al., 2005), also inhibits SCIN activity. MFA produced an XE991-resistant
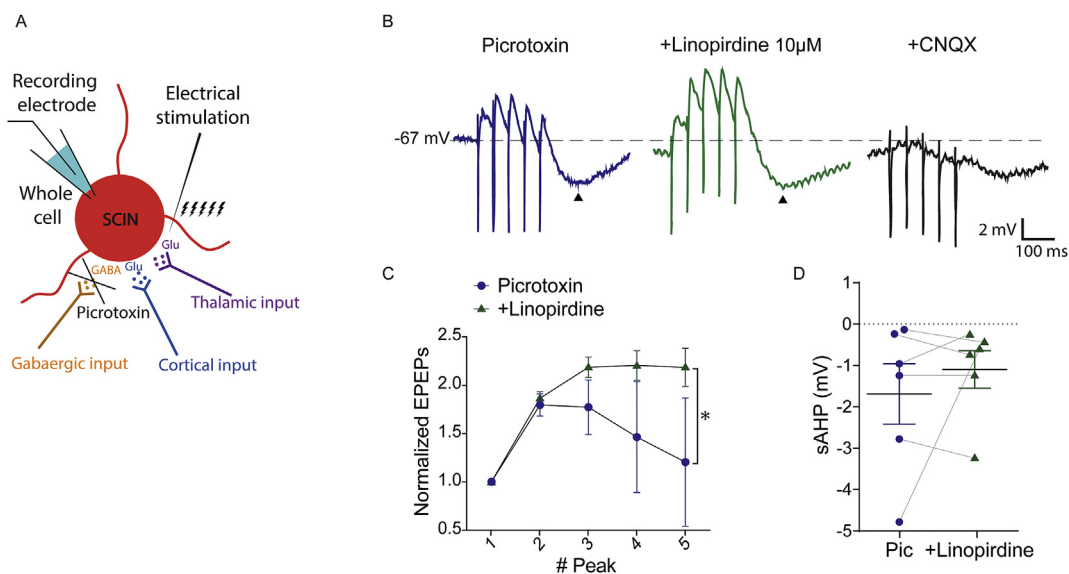
Fig. 5. Linopirdine enhances synaptic temporal integration of SCIN responses to electrical stimulation. A. Schematic diagram of whole cell recordings of EPSPs induced by locally stimulating striatal afferents. **B.** Representative responses of a SCIN to afferent stimulation (5 pulses at 20 Hz) before (blue) and after (green) adding linopirdine (10 μM) to the bath. Addition of CNQX (40 μM) blocked the response to stimulation. **C.** Average normalized EPSP amplitude in control conditions and in the presence of linopirdine. **D.** Average amplitude of the sAHP measured at the point indicated by the arrowhead in B. Statistical analysis: two-way RM-ANOVA with drug treatment and EPSP number as factors [*p = 0.0459, $F_{interaction}(4,20) = 2.944$, n = 6]. (For interpretation of the references to color in this figure legend, the reader is referred to the Web version of this article.)
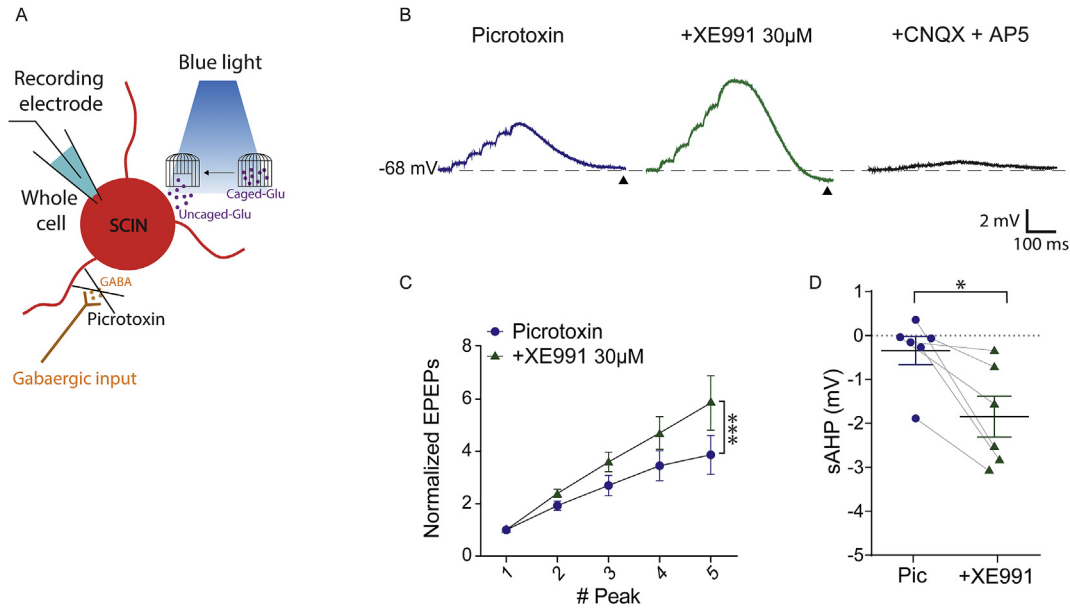
Fig. 6. XE991 enhances synaptic temporal integration of SCIN responses to glutamate uncaging. A. Schematic diagram of whole cell recording of EPSPs induced by locally uncaging glutamate with blue light. **B.** Representative responses of a SCIN to uncaged glutamate (5 light pulses at 20 Hz) before (blue) and after (green) adding XE991 (30 µM) to the bath. Addition of glutamatergic receptor antagonists blocked the response to stimulation. CNQX and AP5 were used at 40 µM and 50 µM, respectively. **C.** Average normalized EPSP amplitude in control conditions and in the presence of XE991. Absolute amplitudes are shown in Fig. S2D. **D.** Average amplitude of the sAHP measured at the point indicated by the arrowhead in B. Statistical analysis: two-way RM-ANOVA with drug treatment and EPSP number as factors [***p = 0.0002, $F_{interaction}(4,20) = 9.271$, n = 6] and paired t-test [*p = 0.0175, t(5) = 3.489, n = 6]. (For interpretation of the references to color in this figure legend, the reader is referred to the Web version of this article.)
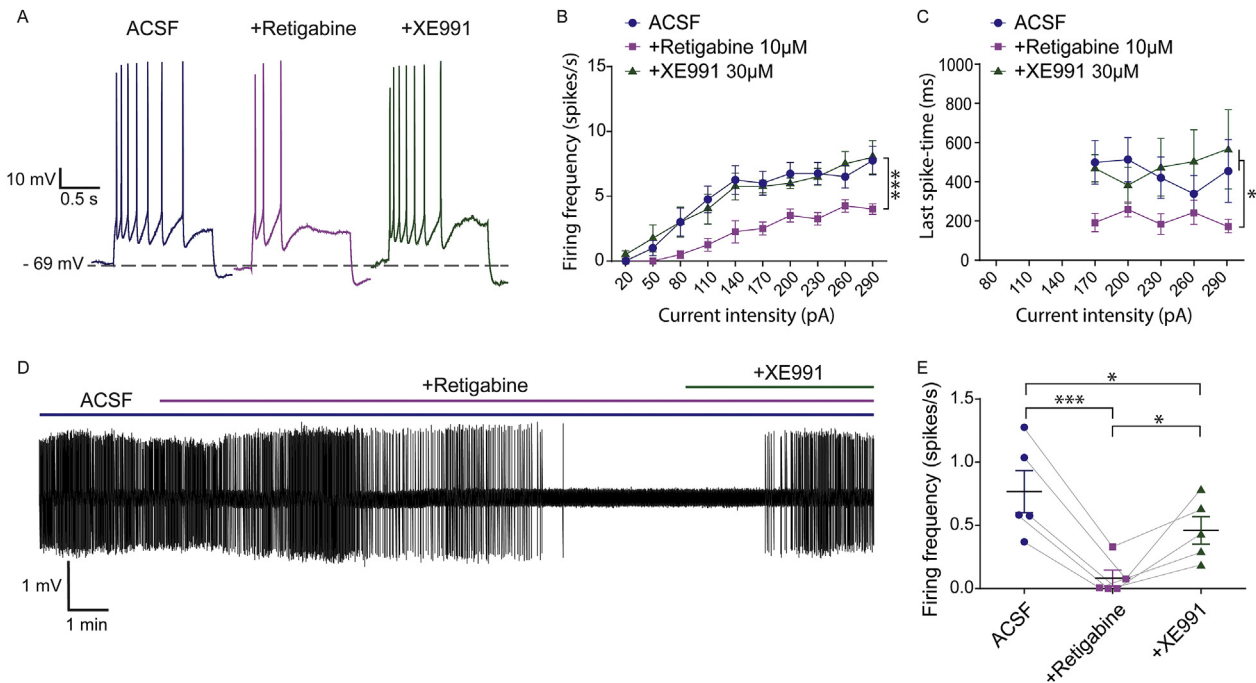
Fig. 7. Kv7 blockade reverts the effect of retigabine. A. Representative response of a SCIN to a depolarizing 140 pA current step before (blue) and after (magenta) adding retigabine (10 µM) to the bath, and reversion (green) of the effect by XE991 (30 µM). **B and C.** Firing frequency (B) and last spike time (C) versus current intensity before and after sequential addition of retigabine and XE991. CNQX and picrotoxin were present in the bath to prevent indirect effects via AMPA and GABA-A receptors. Statistical analysis: two-way RM-ANOVA with drug treatment and current intensity as factors [**B:** ***p = 0.0008, $F_{interaction}(18, 54) = 3.041$, n = 4; **C:** *p = 0.0398, $F_{treatment}(2, 6) = 5.787$, n = 4]. In C data from low intensity pulses were excluded to keep cells with spikes at all intensities. **D.** Representative cell attached recording of SCIN tonic firing in the presence of CNQX and picrotoxin in the bath, before and after sequentially adding retigabine (10 µM) and XE991 (30 µM) to the bath. **E.** Average spontaneous firing frequency of SCIN in control conditions and after the addition of retigabine and XE991. Statistical analysis: one-way RM-ANOVA [F(2, 8) = 22.33, p = 0.0005, n = 5; post-hoc tests (Tukey): ***p = 0.0004, *p = 0.0412 (ACSF vs. XE991) and p = 0.0152 (XE991 vs. retigabine)]. Data are mean ± SEM from at least 3 mice. (For interpretation of the references to color in this figure legend, the reader is referred to the Web version of this article.)

reduction of SCIN excitability that was indistinguishable from the one observed for diclofenac (Fig. 8G–I). Taken together, the results indicate that diclofenac and MFA regulate SCIN excitability through a mechanism different than the one targeted by retigabine (Tables 2–4).

4. Discussion

As many other neurons, SCIN display spike discharge accommodation during sustained depolarization owing to slowly activating K⁺ currents that produce a slow AHP after long excitation (Jiang and North, 1991; Calabresi et al., 1998; Sanchez et al., 2011; Tubert et al., 2016). Classical studies link the M-current (Madison and Nicoll, 1984) and Kv7 channels (Peters et al., 2005) to these features in hippocampal neurons and sympathetic ganglia cholinergic neurons (Adams et al., 1982). Here we showed that the main Kv7 subunits known to contribute to M-current in the brain, Kv7.2 and Kv7.3, are expressed by a large proportion of SCIN, both at the mRNA and protein levels. Kv7.5, which has also a widespread brain expression (Lerche et al., 2000; Jensen et al., 2005) and has been related to sAHP in hippocampal neurons (Tzingounis et al., 2010), is also expressed by SCIN. These data confirm previous reports of Kv7.2 expression by SCIN (Cooper et al., 2001) and other striatal neurons (Martire et al., 2007), and the lack of expression of Kv7.4 in the striatum (Hansen et al., 2017).

Using a battery of Kv7 blockers, we ruled out the involvement of these channels in SCIN spike discharge accommodation and sAHP. This confirmed and expanded our previous reports showing that Kv1 channels are key to these SCIN excitability traits (Tubert et al., 2016) and reports of others showing a prominent Ca²⁺-dependent component of sAHP (Goldberg and Wilson, 2005). Moreover, Kv7 blockers did not change the SCIN resting membrane potential and the frequency of SCIN autonomous pacemaking activity. Instead, we found a very specific effect of Kv7 blockers on EPSP summation. Despite the restricted effect of blockers to synaptic integration, the Kv7 channel opener reduced the excitability and spontaneous firing frequency of SCIN. Thus, although SCIN Kv7 channels seem to be primarily involved in synaptic integration, SCIN Kv7 channels are potentially capable of regulating their somatic excitability and autonomous activity.

A dissociation between the effects of Kv7 channel openers and blockers has previously been reported in studies of other neurons (Hönigsperger et al., 2015; Lombardo and Harrington, 2016). For instance, retigabine diminishes spinal motoneuron excitability by hyperpolarizing their resting membrane potential, reducing their input resistance and depolarizing their action potential threshold, while XE991 only hyperpolarizes the action potential threshold (Lombardo and Harrington, 2016). The authors proposed that the

fraction of Kv7 channels that are active in spinal motoneurons under standard slice physiology study conditions, and are then susceptible to XE991 (Greene et al., 2017), is small, while the whole channel reserve is susceptible to retigabine. Additionally, it has been shown that retigabine can overcome inhibition of Kv7 currents in peripheral sensory neurons (Linley et al., 2012). In our experiments retigabine reduced SCIN excitability (as shown by reduced firing frequency and last spike time, increased rheobase and a more depolarized threshold during depolarizing current injection) and abolished autonomous pacemaking, whereas Kv7 blockers largely failed to modify these SCIN features. Thus, SCIN also have a high reserve of Kv7 channels that are susceptible of recruitment by modulators.

Our data show that Kv7 channels impose a limit to summation of EPSPs evoked by electrical stimulation of SCIN afferents. The limit to summation of subthreshold depolarizations was observed even when the responses were elicited with light-evoked uncaging of glutamate, indicating that Kv7 channels expressed in the postsynaptic side are sufficient for this function. A role for Kv7 channels in shaping subthreshold depolarizations through both pre- and post-synaptic effects was reported in several other neuron types (Shen et al., 2005; Hu et al., 2007; Hönigsperger et al., 2015; Pérez-Ramírez et al., 2015). However, ours is one of the few reports in which a physiological role of Kv7 in EPSP integration is dissociated from a role in action potential firing (Hönigsperger et al., 2015). A plausible explanation of this dissociation could be that, during the intrinsic depolarization that governs autonomous firing, action potential discharge occurs before the Kv7 current gains influence over the membrane potential. Moreover, Kv7 channels can have different roles in different neuronal compartments or localize to a specific compartment which in most reports is close to the action potential initiation site and nodes of Ranvier (Devaux et al., 2004; Yue and Yaari, 2006; Battefeld et al., 2014). Axonal initial segment localization of Kv7.2 and Kv7.3 requires an anchor motif through which these subunits interact with ankyrin-G (Cooper, 2011). The Kv7.5 subunit lacks this anchor, suggesting a more widespread distribution of Kv7 channels in SCIN.

Interestingly, the amplitude of the sAHP that follows the EPSP train could be enhanced rather than reduced after Kv7 channel blockade, likely because the higher EPSP summation results in an enhanced recruitment of the currents mediating the sAHP. This is also consistent with our previous findings showing that Kv1.3 channel blockade reduces the sAHP that follows an EPSP train in SCIN (Tubert et al., 2016) and suggests that a fine regulation of Kv channels would allow an independent regulation of EPSP integration and sAHP amplitude. Given that an enhancement of the sAHP was observed following EPSPs evoked by glutamate uncaging and not after electrical stimulation, we cannot rule out the possibility that neurotransmitters other than glutamate are released by the stimulus and exert a negative modulation of the sAHP (Klink and Alonso, 1997; Lancaster et al., 2001; Satake et al., 2008).

Diclofenac behaves as a Kv7 channel opener when the channels are composed of Kv7.2, Kv7.3 and Kv7.4 subunits, but it inhibits the current carried by Kv7.5 homomeric channels and Kv7.5/Kv7.4 heteromeric channels (Peretz et al., 2005; Brueggemann et al., 2011). Kv7.5 seems to not form channels with Kv7.2, but it makes channels with Kv7.3 (Lerche et al., 2000; Wickenden et al., 2001; Bal et al., 2008); the effect of diclofenac on Kv7.5/Kv7.3 channels remains unknown. We speculated that diclofenac could be used to interrogate the prevalent composition of Kv7 channels in SCIN (see Brueggemann et al., 2011); if most SCIN channels were composed of Kv7.2 and Kv7.3 subunits, as it is commonly the case in central neurons (Wang et al., 1998; Brown and Passmore, 2009), diclofenac would diminish SCIN excitability and autonomous firing. Although it proved to be effective to do so, unexpectedly, the inhibitory effect

Table 2
Comparison of SCIN electrophysiological features before and after Retigabine. The recordings were performed in the presence of 100 μM picrotoxin and 40 μM CNQX. Retigabine was used at 10 μM. The values represent the mean ± SEM (n = 8). Statistical test: Wilcoxon, except for input resistance which used a slope comparison in linear regression analysis from graphpad software.

Property	ACSF	Retigabine	p value
Resting membrane potential (mV)	−67.8 ± 1.16	−67.9 ± 1.25	0.8438
Input resistance (MΩ)	120.7 ± 6.2	127.5 ± 8.8	0.5480
Sag amplitude (mV)	2.9 ± 0.75	3.6 ± 0.86	0.4609
Sag latency (ms)	77.7 ± 7.15	83.5 ± 11.15	0.9453
sAHP amplitude (mV)	7.2 ± 1.27	7.6 ± 1.23	0.9453
Rheobase (pA)	68.8 ± 11.25	102.5 ± 15.59	**0.0313**
Threshold (mV)	−43.8 ± 0.77	−41.3 ± 0.87	**0.0078**
Amplitude of 1st spike (mV)	73.7 ± 2.37	70.4 ± 3.6	0.3828
Width of 1st spike (ms)	1.4 ± 0.08	1.6 ± 0.15	0.1563
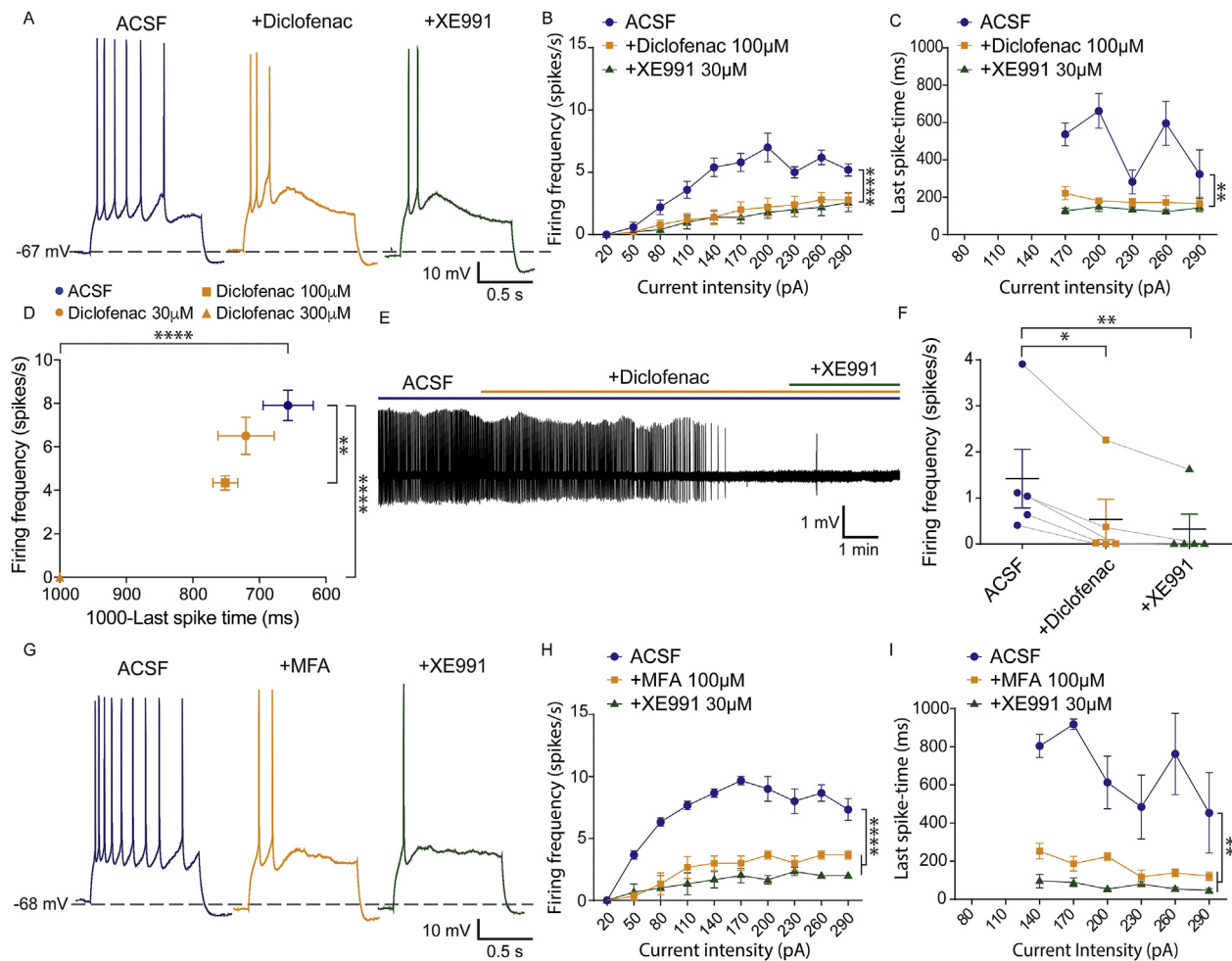
Fig. 8. Kv7 blockade does not revert the effect of diclofenac on SCIN firing properties. A. Representative responses of a SCIN to a depolarizing 140 pA current step before (blue) and after (yellow) adding diclofenac (100 μM) to the bath, and lack of reversion (green) after adding XE991 (30 μM). B and C. Firing frequency (B) and last spike time (C) versus current intensity before and after sequential addition of diclofenac (100 μM) and XE991 (30 μM). CNQX and picrotoxin were present in the bath to prevent indirect effects via AMPA and GABA-A receptor. Statistical analysis: two-way RM-ANOVA with drug treatment and current intensity as factors [B: ****p < 0.0001, $F_{interaction}(18, 72) = 10.22$, n = 5; C: **p = 0.0071, $F_{interaction}(8, 24) = 3.588$, n = 4]. In C data from low intensity pulses were excluded to keep cells with spikes at all intensities. D. Firing frequency vs. time after last spike (for cases with no spikes the pulse duration was considered as a cutoff value) in response to a 230 pA depolarizing current step before and after addition of diclofenac 30, 100 or 300 μM. Statistical analysis: two-way RM-ANOVA with concentration and current intensity as factors [Only the current intensity was considered as RM; effects on firing frequency: $F_{interaction}(27,144) = 11.25$, $F_{treatment}(3,16) = 12.24$; effects on time after last spike: $F_{treatment}(3,16) = 11.22$; n = 3–4 cells from 3 animals per condition; **p = 0.0041, ****p < 0.0001, post-hoc tests for the 230 pA pulse]. E. Representative cell attached recording of a SCIN tonic firing in the presence of CNQX and picrotoxin in the bath, before and after sequentially adding diclofenac (100 μM) and XE991 (30 μM) to the bath. F. Average spontaneous firing frequency of SCIN in control conditions and after the addition of diclofenac and XE991. Statistical analysis: one-way RM-ANOVA [F(2, 8) = 11.9, p = 0.0040, n = 5 from 3 mice; post-hoc tests (Tukey): *p = 0.0145, **p = 0.0044]. G. Representative responses of a SCIN to depolarizing current steps before (blue) and after (yellow) adding meclofenamic acid (100 μM) to the bath, and lack of reversion (green) after adding XE991 (30 μM). H and I. Firing frequency (H) and last spike time (I) versus current intensity before and after sequential addition of MFA (100 μM) and XE991 (30 μM). CNQX and picrotoxin were present in the bath to prevent indirect effects via AMPA and GABA-A receptor. Statistical analysis: two-way RM-ANOVA with drug treatment and current intensity as factors [H: ****p < 0.0001, $F_{interaction}(18, 36) = 11.54$, n = 3; I: **p = 0.0085, $F_{treatment}(2, 4) = 19.75$, n = 3]. In I data from low intensity pulses were excluded to keep cells with spikes at all intensities. Data are mean ± SEM. (For interpretation of the references to color in this figure legend, the reader is referred to the Web version of this article.)

of diclofenac could not be reverted by the Kv7 blocker XE991, in contrast to what was observed here for retigabine and in contrast with reports in thalamocortical neurons, where diclofenac enhancement of the M-current was blocked and prevented by XE991 (Cerina et al., 2015). The lack of reversion of the effect of diclofenac and MFA suggests that these drugs act through a Kv7-independent mechanism. In addition to the M-current, diclofenac can modify other neuronal ion channels through direct or indirect effects (Voilley et al., 2001; Liu et al., 2005; Villalonga et al., 2010; Huang et al., 2013; Sun et al., 2017).

EPSP integration might shape the response of SCIN to salient environmental events. During instrumental learning SCIN develop a response to rewards and reward-predictive stimuli consisting in a brief excitation followed by a transient inhibition or "pause" lasting

around 200 ms, which is usually followed by another excitation (Kimura et al., 1984; Aosaki et al., 1994). SCIN can also show a similar response to salient unexpected events (Apicella et al., 1997). There is evidence that the initial brief excitation is induced by excitatory afferents coming from the thalamus (Matsumoto et al., 2001), but cortical afferents might also evoke similar responses in SCIN (Reynolds et al., 2004). An interesting observation is that these SCIN responses are not invariable in the same SCIN to different stimuli or across the SCIN population to the same stimulus; the initial action potential discharge might not be present and the pause latency, intensity and duration can vary with different stimuli (reviewed by Zhang and Cragg, 2017). Among a diversity of mechanisms, intrinsic potassium currents initiated by a synaptically-induced excitation were proposed as the underlying

Table 3
Comparison of SCIN electrophysiological features before and after diclofenac. The recordings were performed in the presence of 100 μM picrotoxin and 40 μM CNQX. Diclofenac was used at 100 μM. The values represent the mean ± SEM (n = 5). Statistical test: Wilcoxon, except for input resistance which used a slope comparison in linear regression analysis from graphpad software.

Property	ACSF	Diclofenac	p value
Resting membrane potential (mV)	−65.2 ± 1.33	−66.7 ± 1.06	0.3125
Input resistance (MΩ)	125.2 ± 9.5	120.8 ± 13.8	0.7957
Sag amplitude (mV)	3.2 ± 0.70	3.0 ± 0.82	0.8532
Sag latency (ms)	81.0 ± 5.20	69.3 ± 6.60	0.0625
sAHP amplitude (mV)	6.9 ± 1.62	6.3 ± 1.22	>0.9999
Rheobase (pA)	68.0 ± 7.35	128.0 ± 38.65	0.5000
Threshold (mV)	−42.1 ± 0.78	−39.6 ± 0.47	0.0625
Amplitude of 1st spike (mV)	76.9 ± 2.91	68.3 ± 4.94	0.0625
Width of 1st spike (ms)	1.3 ± 0.08	1.4 ± 0.1	0.1250

Table 4
Comparison of SCIN electrophysiological features before and after meclofenamic acid. The recordings were performed in the presence of 100 μM picrotoxin and 40 μM CNQX. MFA was used at 100 μM. The values represent the mean ± SEM (n = 3). Statistical test: Wilcoxon, except for input resistance which used a slope comparison in linear regression analysis from graphpad software.

Property	ACSF	MFA	p value
Resting membrane potential (mV)	−66.9 ± 1.28	−67.6 ± 0.86	>0.9999
Input resistance (MΩ)	127.9 ± 8.6	104.3 ± 25.1	0.4005
Sag amplitude (mV)	3.3 ± 0.69	3.2 ± 0.81	>0.9999
Sag latency (ms)	82.9 ± 11.99	66.5 ± 2.68	0.2500
sAHP amplitude (mV)	6.8 ± 1.02	6.2 ± 0.90	0.7500
Rheobase (pA)	50.0 ± 0.0	70.0 ± 20.00	>0.9999
Threshold (mV)	−40.5 ± 1.40	−36.9 ± 1.09	0.2500
Amplitude of 1st spike (mV)	66.0 ± 4.09	60.5 ± 3.84	0.2500
Width of 1st spike (ms)	1.8 ± 0.06	2.1 ± 0.17	0.2500

mechanism of the pause response, which has been compared to a sAHP (Reynolds et al., 2004). Our results show that SCIN Kv7 channels can be recruited by afferent stimulation to limit EPSP summation but do not contribute significantly to the sAHP. Other currents, including Kv1.3 and KCa currents, may be more important determinants of the sAHP in SCIN (Goldberg and Wilson, 2005; Tubert et al., 2016). Altogether, the data available suggest that differential expression and regulation of Kv currents may be a factor contributing to the diversity of SCIN responses to salient events. Additionally, because dopamine receptors can functionally couple to Kv7 channels (Ljungstrom et al., 2003) and modulate neuronal activity through Kv7-dependent mechanisms (Choi et al., 2017), and the response of SCIN to salient events is modulated by dopamine receptors (Watanabe and Kimura, 1998), future studies will focus on Kv7 channels as possible contributors to the features of the SCIN pause response in normal and pathological conditions. Finally, the data presented here brings attention towards Kv7 channel-related and NSAID pharmacological tools as putative modulators of SCIN activity in pathological conditions characterized by SCIN activity dysregulation like Parkinson's disease and ʟ-DOPA-induced dyskinesia.

Declarations of interest

None.

Acknowledgments

Appendix A. Supplementary data

Supplementary data related to this article can be found at https://doi.org/10.1016/j.neuropharm.2018.05.010.

References

Adams, P.R., Brown, D.A., Constanti, A., 1982. Pharmacological inhibition of the M-current. J. Physiol. 332, 223–262. Available at: http://www.ncbi.nlm.nih.gov/pubmed/6760380. (Accessed 5 January 2018).

Aldrin-Kirk, P., Heuer, A., Rylander Ottosson, D., Davidsson, M., Mattsson, B., Björklund, T., 2018. Chemogenetic modulation of cholinergic interneurons reveals their regulating role on the direct and indirect output pathways from the striatum. Neurobiol. Dis. 109, 148–162. Available at: http://linkinghub.elsevier.com/retrieve/pii/S096999611730236X. (Accessed 2 January 2018).

Aliane, V., Pérez, S., Bohren, Y., Deniau, J.-M., Kemel, M.-L., 2011. Key role of striatal cholinergic interneurons in processes leading to arrest of motor stereotypies. Brain 134, 110–118. Available at: https://academic.oup.com/brain/article-lookup/doi/10.1093/brain/awq285. (Accessed 2 January 2018).

Aosaki, T., Graybiel, A.M., Kimura, M., 1994. Effect of the nigrostriatal dopamine system on acquired neural responses in the striatum of behaving monkeys. Science 265, 412–415. Available at: http://www.ncbi.nlm.nih.gov/pubmed/8023166. (Accessed 8 July 2015).

Apicella, P., Legallet, E., Trouche, E., 1997. Responses of tonically discharging neurons in the monkey striatum to primary rewards delivered during different behavioral states. Exp. Brain Res. 116, 456–466. Available at: http://www.ncbi.nlm.nih.gov/pubmed/9372294. (Accessed 25 January 2018).

Atherton, J.F., Bevan, M.D., 2005. Ionic mechanisms underlying autonomous action potential generation in the somata and dendrites of GABAergic substantia nigra pars reticulata neurons in vitro. J. Neurosci. 25, 8272–8281. Available at: http://www.ncbi.nlm.nih.gov/pubmed/16148235. (Accessed 2 January 2018).

Bal, M., Zhang, J., Zaika, O., Hernandez, C.C., Shapiro, M.S., 2008. Homomeric and heteromeric assembly of KCNQ (Kv7) K $^{+}$ channels assayed by total internal reflection fluorescence/fluorescence resonance energy transfer and patch clamp analysis. J. Biol. Chem. 283, 30668–30676. Available at: http://www.ncbi.nlm.nih.gov/pubmed/18786918. (Accessed 10 January 2018).

Battefeld, A., Tran, B.T., Gavrilis, J., Cooper, E.C., Kole, M.H.P., 2014. Heteromeric Kv7.2/7.3 channels differentially regulate action potential initiation and conduction in neocortical myelinated axons. J. Neurosci. 34, 3719–3732. Available at: http://www.ncbi.nlm.nih.gov/pubmed/24599470. (Accessed 2 January 2018).

Bennett, B.D., Wilson, C.J., 1999. Spontaneous activity of neostriatal cholinergic interneurons in vitro. J. Neurosci. 19, 5586–5596. Available at: http://www.ncbi.nlm.nih.gov/pubmed/10377365. (Accessed 2 January 2018).

Bordia, T., Perez, X.A., Heiss, J.E., Zhang, D., Quik, M., 2016. Optogenetic activation of striatal cholinergic interneurons regulates L-dopa-induced dyskinesias. Neurobiol. Dis. 91, 47–58. Available at: http://www.ncbi.nlm.nih.gov/pubmed/26921469. (Accessed 27 December 2017).

Bradfield, L.A., Bertran-Gonzalez, J., Chieng, B., Balleine, B.W., 2013. The thalamostriatal pathway and cholinergic control of goal-directed action: interlacing new with existing learning in the striatum. Neuron 79, 153–166. Available at: http://linkinghub.elsevier.com/retrieve/pii/S089662731300370X. (Accessed 2 January 2018).

Braz, B.Y., Galiñanes, G.L., Taravini, I.R., Belforte, J.E., Murer, M.G., 2015. Altered corticostriatal connectivity and exploration-exploitation imbalance emerge as intermediate phenotypes for a neonatal dopamine dysfunction. Neuropsychopharmacology. Available at: http://www.ncbi.nlm.nih.gov/pubmed/25872916. (Accessed 29 April 2015).

Brown, A.R., Hu, B., Antle, M.C., Teskey, G.C., 2009. Neocortical movement representations are reduced and reorganized following bilateral intrastriatal 6-hydroxydopamine infusion and dopamine type-2 receptor antagonism. Exp. Neurol. 220, 162–170. Available at: http://www.ncbi.nlm.nih.gov/pubmed/19703443. (Accessed 14 December 2017).

Brown, D.A., 2017. Regulation of neural ion channels by muscarinic receptors. Neuropharmacology. Available at: http://www.ncbi.nlm.nih.gov/pubmed/29154951. (Accessed 2 January 2018).

Brown, D.A., Passmore, G.M., 2009. Neural KCNQ (Kv7) channels. Br. J. Pharmacol. 156, 1185–1195. Available at: http://www.ncbi.nlm.nih.gov/pubmed/19298256. (Accessed 2 January 2018).

Brueggemann, L.I., Mackie, A.R., Martin, J.L., Cribbs, L.L., Byron, K.L., 2011. Diclofenac distinguishes among homomeric and heteromeric potassium channels composed of KCNQ4 and KCNQ5 subunits. Mol. Pharmacol. 79, 10–23. Available at: http://www.pubmedcentral.nih.gov/articlerender.fcgi?artid=3014280&tool=pmcentrez&rendertype=abstract. (Accessed 3 July 2015).

Calabresi, P., Centonze, D., Pisani, A., Sancesario, G., North, R.A., Bernardi, G., 1998. Muscarinic IPSPs in rat striatal cholinergic interneurones. J. Physiol. 510 (Pt 2),

421—427. Available at: http://www.ncbi.nlm.nih.gov/pubmed/9705993. (Accessed 5 January 2018).

Cerina, M., Szkudlarek, H.J., Coulon, P., Meuth, P., Kanyshkova, T., Nguyen, X.V., Göbel, K., Seidenbecher, T., Meuth, S.G., Pape, H.-C., Budde, T., 2015. Thalamic Kv 7 channels: pharmacological properties and activity control during noxious signal processing. Br. J. Pharmacol. 172, 3126—3140. Available at: http://www.ncbi.nlm.nih.gov/pubmed/25684311. (Accessed 5 January 2018).

Choi, S.J., Mukai, J., Kvajo, M., Xu, B., Diamantopoulou, A., Pitychoutis, P.M., Gou, B., Gogos, J.A., Zhang, H., 2017. A schizophrenia-related deletion leads to KCNQ2-dependent abnormal dopaminergic modulation of prefrontal cortical interneuron activity. Cerebr. Cortex 1—17. Available at: https://academic.oup.com/cercor/article-lookup/doi/10.1093/cercor/bhx123. (Accessed 23 January 2018).

Cooper, E.C., 2011. Made for "anchorin": Kv7.2/7.3 (KCNQ2/KCNQ3) channels and the modulation of neuronal excitability in vertebrate axons. Semin. Cell Dev. Biol. 22, 185—192. Available at: http://www.ncbi.nlm.nih.gov/pubmed/20940059. (Accessed 2 January 2018).

Cooper, E.C., Harrington, E., Jan, Y.N., Jan, L.Y., 2001. M channel KCNQ2 subunits are localized to key sites for control of neuronal network oscillations and synchronization in mouse brain. J. Neurosci. 21, 9529—9540. Available at: http://www.ncbi.nlm.nih.gov/pubmed/11739564. (Accessed 2 July 2015).

Cragg, S.J., 2006. Meaningful silences: how dopamine listens to the ACh pause. Trends Neurosci. 29, 125—131. Available at: http://www.ncbi.nlm.nih.gov/pubmed/16443285. (Accessed 9 July 2015).

Deng, P., Zhang, Y., Xu, Z.C., 2007. Involvement of I(h) in dopamine modulation of tonic firing in striatal cholinergic interneurons. J. Neurosci. 27, 3148—3156. Available at: http://www.ncbi.nlm.nih.gov/pubmed/17376976. (Accessed 13 July 2015).

Devaux, J.J., Kleopa, K.A., Cooper, E.C., Scherer, S.S., 2004. KCNQ2 is a nodal K+ channel. J. Neurosci. 24, 1236—1244. Available at: http://www.ncbi.nlm.nih.gov/pubmed/14762142. (Accessed 10 January 2018).

Ding, J.B., Guzman, J.N., Peterson, J.D., Goldberg, J.A., Surmeier, D.J., 2010. Thalamic gating of corticostriatal signaling by cholinergic interneurons. Neuron 67, 294—307. Available at: http://www.pubmedcentral.nih.gov/articlerender.fcgi?artid=4085694&tool=pmcentrez&rendertype=abstract. (Accessed 11 July 2014).

Fino, E., Araya, R., Peterka, D.S., Salierno, M., Etchenique, R., Yuste, R., 2009. RuBi-glutamate: two-photon and visible-light photoactivation of neurons and dendritic spines. Front. Neural Circ. 3, 2. Available at: http://journal.frontiersin.org/article/10.3389/neuro.04.002.2009/abstract. (Accessed 2 January 2018).

Goldberg, J.A., Wilson, C.J., 2005. Control of spontaneous firing patterns by the selective coupling of calcium currents to calcium-activated potassium currents in striatal cholinergic interneurons. J. Neurosci. 25, 10230—10238. Available at: http://www.pubmedcentral.nih.gov/articlerender.fcgi?artid=1343481&tool=pmcentrez&rendertype=abstract. (Accessed 7 July 2015).

Greene, D.L., Kang, S., Hoshi, N., 2017. XE991 and linopirdine are state-dependent inhibitors for Kv7/KCNQ channels that favor activated single subunits. J. Pharmacol. Exp. Therapeut. 362, 177—185. Available at: http://www.ncbi.nlm.nih.gov/pubmed/28483800. (Accessed 10 January 2018).

Hansen, H.H., Weikop, P., Mikkelsen, M.D., Rode, F., Mikkelsen, J.D., 2017. The pan-Kv7 (KCNQ) channel opener retigabine inhibits striatal excitability by direct action on striatal neurons In Vivo. Basic Clin. Pharmacol. Toxicol. 120, 46—51. Available at: http://doi.wiley.com/10.1111/bcpt.12636. (Accessed 5 January 2018).

Hönigsperger, C., Marosi, M., Murphy, R., Storm, J.F., 2015. Dorsoventral differences in Kv7/M-current and its impact on resonance, temporal summation and excitability in rat hippocampal pyramidal cells. J. Physiol. 593, 1551—1580. Available at: http://doi.wiley.com/10.1113/jphysiol.2014.280826. (Accessed 3 January 2018).

Hu, H., Vervaeke, K., Storm, J.F., 2002. Two forms of electrical resonance at theta frequencies, generated by M-current, h-current and persistent Na+ current in rat hippocampal pyramidal cells. J. Physiol. 545, 783—805. Available at: http://www.ncbi.nlm.nih.gov/pubmed/12482886. (Accessed 3 January 2018).

Hu, H., Vervaeke, K., Storm, J.F., 2007. M-Channels (Kv7/KCNQ channels) that regulate synaptic integration, excitability, and spike pattern of CA1 pyramidal cells are located in the perisomatic region. J. Neurosci. 27, 1853—1867. Available at: http://www.ncbi.nlm.nih.gov/pubmed/17314282. (Accessed 4 January 2018).

Huang, C.W., Hung, T.Y., Liao, Y.K., Hsu, M.C., Wu, S.N., 2013. Underlying mechanism of regulatory actions of diclofenac, a nonsteroidal anti-inflammatory agent, on neuronal potassium channels and firing: an experimental and theoretical study. J. Physiol. Pharmacol. 64, 269—280. Available at: http://www.ncbi.nlm.nih.gov/pubmed/23959723. (Accessed 5 January 2018).

Huang, H., Trussell, L.O., 2011. KCNQ5 channels control resting properties and release probability of a synapse. Nat. Neurosci. 14, 840—847. Available at: http://www.nature.com/doifinder/10.1038/nn.2830. (Accessed 2 January 2018).

Jensen, H.S., Callø, K., Jespersen, T., Jensen, B.S., Olesen, S.-P., 2005. The KCNQ5 potassium channel from mouse: a broadly expressed M-current like potassium channel modulated by zinc, pH, and volume changes. Mol. Brain Res. 139, 52—62. Available at: http://www.ncbi.nlm.nih.gov/pubmed/15963599. (Accessed 19 January 2018).

Jentsch, T.J., 2000. Neuronal KCNQ potassium channels: physiology and role in disease. Nat. Rev. Neurosci. 1, 21—30. Available at: http://www.ncbi.nlm.nih.gov/pubmed/11252765. (Accessed 2 January 2018).

Jiang, Z.G., North, R.A., 1991. Membrane properties and synaptic responses of rat striatal neurones in vitro. J. Physiol. 443, 533—553. Available at: http://www.ncbi.nlm.nih.gov/pubmed/1822537. (Accessed 2 January 2018).

Kalia, L.V., Lang, A.E., 2015. Parkinson's disease. Lancet. Available at: http://www.ncbi.nlm.nih.gov/pubmed/25904081. (Accessed 20 April 2015).

Kharkwal, G., Brami-Cherrier, K., Lizardi-Ortiz, J.E., Nelson, A.B., Ramos, M., Del Barrio, D., Sulzer, D., Kreitzer, A.C., Borrelli, E., 2016. Parkinsonism driven by antipsychotics originates from dopaminergic control of striatal cholinergic interneurons. Neuron 91, 67—78. Available at: http://linkinghub.elsevier.com/retrieve/pii/S0896627316302677. (Accessed 2 January 2018).

Kimura, M., Rajkowski, J., Evarts, E., 1984. Tonically discharging putamen neurons exhibit set-dependent responses. Proc. Natl. Acad. Sci. U. S. A. 81, 4998—5001. Available at: http://www.ncbi.nlm.nih.gov/pubmed/6589643. (Accessed 24 January 2018).

Klink, R., Alonso, A., 1997. Muscarinic modulation of the oscillatory and repetitive firing properties of entorhinal cortex layer II neurons. J. Neurophysiol. 77 (4), 1813—1828.

Lancaster, B., Hu, H., Ramakers, G.M., Storm, J.F., 2001. Interaction between synaptic excitation and slow afterhyperpolarization current in rat hippocampal pyramidal cells. J. Physiol. 536 (Pt 3), 809—823.

Lee, S., Kwag, J., 2012. M-channels modulate the intrinsic excitability and synaptic responses of layer 2/3 pyramidal neurons in auditory cortex. Biochem. Biophys. Res. Commun. 426, 448—453. Available at: http://linkinghub.elsevier.com/retrieve/pii/S0006291X12015677. (Accessed 3 January 2018).

Lerche, C., Scherer, C.R., Seebohm, G., Derst, C., Wei, A.D., Busch, A.E., Steinmeyer, K., 2000. Molecular cloning and functional expression of KCNQ5, a potassium channel subunit that may contribute to neuronal m-current diversity. J. Biol. Chem. 275, 22395—22400. Available at: http://www.ncbi.nlm.nih.gov/pubmed/10787416. (Accessed 19 January 2018).

Linley, J.E., Pettinger, L., Huang, D., Gamper, N., 2012. M channel enhancers and physiological M channel block. J. Physiol. 590, 793—807. Available at: http://www.ncbi.nlm.nih.gov/pubmed/22155935. (Accessed 15 January 2018).

Liu, L.-Y., Fei, X.-W., Li, Z.-M., Zhang, Z.-H., Mei, Y.-A., 2005. Diclofenac, a nonsteroidal anti-inflammatory drug, activates the transient outward K+ current in rat cerebellar granule cells. Neuropharmacology 48, 918—926. Available at: http://www.ncbi.nlm.nih.gov/pubmed/15829261. (Accessed 15 January 2018).

Ljungstrom, T., Grunnet, M., Jensen, B.S., Olesen, S.-P., 2003. Functional coupling between heterologously expressed dopamine D(2) receptors and KCNQ channels. Pflügers Archiv 446, 684—694. Available at: http://link.springer.com/10.1007/s00424-003-1111-2. (Accessed 25 January 2018).

Lombardo, J., Harrington, M.A., 2016. Nonreciprocal mechanisms in up- and downregulation of spinal motoneuron excitability by modulators of KCNQ/Kv 7 channels. J. Neurophysiol. 116, 2114—2124. Available at: http://www.ncbi.nlm.nih.gov/pubmed/27512022. (Accessed 8 January 2018).

Madisen, L., Zwingman, T.A., Sunkin, S.M., Oh, S.W., Zariwala, H.A., Gu, H., Ng, L.L., Palmiter, R.D., Hawrylycz, M.J., Jones, A.R., Lein, E.S., Zeng, H., 2010. A robust and high-throughput Cre reporting and characterization system for the whole mouse brain. Nat. Neurosci. 13, 133—140. Available at: http://www.pubmedcentral.nih.gov/articlerender.fcgi?artid=2840225&tool=pmcentrez&rendertype=abstract. (Accessed 10 July 2014).

Madison, D.V., Nicoll, R.A., 1984. Control of the repetitive discharge of rat CA 1 pyramidal neurones in vitro. J. Physiol. 354, 319—331. Available at: http://www.pubmedcentral.nih.gov/articlerender.fcgi?artid=1193414&tool=pmcentrez&rendertype=abstract. (Accessed 2 July 2015).

Main, M.J., Cryan, J.E., Dupere, J.R., Cox, B., Clare, J.J., Burbidge, S.A., 2000. Modulation of KCNQ2/3 potassium channels by the novel anticonvulsant retigabine. Mol. Pharmacol. 58, 253—262. Available at: http://www.ncbi.nlm.nih.gov/pubmed/10908292. (Accessed 8 January 2018).

Martire, M., D'Amico, M., Panza, E., Miceli, F., Viggiano, D., Lavergata, F., Iannotti, F.A., Barrese, V., Preziosi, P., Annunziato, L., Taglialatela, M., 2007. Involvement of KCNQ2 subunits in [3H]dopamine release triggered by depolarization and presynaptic muscarinic receptor activation from rat striatal synaptosomes. J. Neurochem. 102 (1), 179—193.

Martos, Y.V., Braz, B.Y., Beccaria, J.P., Murer, M.G., Belforte, J.E., 2017. Compulsive social behavior emerges after selective ablation of striatal cholinergic interneurons. J. Neurosci. 37, 2849—2858. Available at: http://www.jneurosci.org/lookup/doi/10.1523/JNEUROSCI.3460-16.2017. (Accessed 2 January 2018).

Matsumoto, N., Minamimoto, T., Graybiel, A.M., Kimura, M., 2001. Neurons in the thalamic CM-Pf complex supply striatal neurons with information about behaviorally significant sensory events. J. Neurophysiol. 85, 960—976. Available at: http://www.ncbi.nlm.nih.gov/pubmed/11160526. (Accessed 12 November 2014).

Maurice, N., Liberge, M., Jaouen, F., Ztaou, S., Hanini, M., Camon, J., Deisseroth, K., Amalric, M., Kerkerian-Le Goff, L., Beurrier, C., 2015. Striatal cholinergic interneurons control motor behavior and basal ganglia function in experimental parkinsonism. Cell Rep. 13, 657—666. Available at: http://www.ncbi.nlm.nih.gov/pubmed/26489458. (Accessed 27 October 2015).

Maurice, N., Mercer, J., Chan, C.S., Hernandez-Lopez, S., Held, J., Tkatch, T., Surmeier, D.J., 2004. D2 dopamine receptor-mediated modulation of voltage-dependent Na+ channels reduces autonomous activity in striatal cholinergic interneurons. J. Neurosci. 24, 10289—10301. Available at: http://www.ncbi.nlm.nih.gov/pubmed/15548642. (Accessed 6 July 2015).

Peretz, A., Degani, N., Nachman, R., Uziyel, Y., Gibor, G., Shabat, D., Attali, B., 2005. Meclofenamic acid and diclofenac, novel templates of KCNQ2/Q3 potassium channel openers, depress cortical neuron activity and exhibit anticonvulsant properties. Mol. Pharmacol. 67, 1053—1066. Available at: http://www.ncbi.nlm.nih.gov/pubmed/15598972. (Accessed 4 January 2018).

Pérez-Ramírez, M.B., Laville, A., Tapia, D., Duhne, M., Lara-González, E., Bargas, J., Galarraga, E., 2015. KV7 channels regulate firing during synaptic integration in GABAergic striatal neurons. Neural Plast. 2015, 472676. Available at: http://www.hindawi.com/journals/np/2015/472676/. (Accessed 3 January 2018).

Peters, H.C., Hu, H., Pongs, O., Storm, J.F., Isbrandt, D., 2005. Conditional transgenic suppression of M channels in mouse brain reveals functions in neuronal excitability, resonance and behavior. Nat. Neurosci. 8, 51—60. Available at: http://www.nature.com/articles/nn1375. (Accessed 2 January 2018).

Pisani, A., Bernardi, G., Ding, J., Surmeier, D.J., 2007. Re-emergence of striatal cholinergic interneurons in movement disorders. Trends Neurosci. 30, 545—553. Available at: http://www.ncbi.nlm.nih.gov/pubmed/17904652. (Accessed 6 July 2015).

Reynolds, J.N.J., Hyland, B.I., Wickens, J.R., 2004. Modulation of an after-hyperpolarization by the substantia nigra induces pauses in the tonic firing of striatal cholinergic interneurons. J. Neurosci. 24, 9870—9877. Available at: http://www.ncbi.nlm.nih.gov/pubmed/15525771. (Accessed 19 January 2018).

Rossi, J., Balthasar, N., Olson, D., Scott, M., Berglund, E., Lee, C.E., Choi, M.J., Lauzon, D., Lowell, B.B., Elmquist, J.K., 2011. Melanocortin-4 receptors expressed by cholinergic neurons regulate energy balance and glucose homeostasis. Cell Metabol. 13, 195—204. Available at: http://www.ncbi.nlm.nih.gov/pubmed/21284986. (Accessed 25 January 2018).

Rossi, S.P., Matzkin, M.E., Terradas, C., Ponzio, R., Puigdomenech, E., Levalle, O., Calandra, R.S., Frungieri, M.B., 2012. New insights into melatonin/CRH signaling in hamster Leydig cells. Gen. Comp. Endocrinol. 178, 153—163. Available at: http://www.ncbi.nlm.nih.gov/pubmed/22580327. (Accessed 25 January 2018).

Sanchez, G., Rodriguez, M.J., Pomata, P., Rela, L., Murer, M.G., 2011. Reduction of an afterhyperpolarization current increases excitability in striatal cholinergic interneurons in rat parkinsonism. J. Neurosci. 31, 6553—6564. Available at: http://www.ncbi.nlm.nih.gov/pubmed/21525296. (Accessed 5 February 2015).

Satake, T., Mitani, H., Nakagome, K., Kaneko, K., 2008. Individual and additive effects of neuromodulators on the slow components of afterhyperpolarization currents in layer V pyramidal cells of the rat medial prefrontal cortex. Brain Res. 1229, 47—60.

Schneider, C.A., Rasband, W.S., Eliceiri, K.W., 2012. NIH Image to ImageJ: 25 years of image analysis. Nat Methods 9, 671—675. Available at: http://www.ncbi.nlm.nih.gov/pubmed/22930834. (Accessed 25 January 2018).

Shen, W., Hamilton, S.E., Nathanson, N.M., Surmeier, D.J., 2005. Cholinergic suppression of KCNQ channel currents enhances excitability of striatal medium spiny neurons. J. Neurosci. 25, 7449—7458. Available at: http://www.ncbi.nlm.nih.gov/pubmed/16093396. (Accessed 3 January 2018).

Soh, H., Tzingounis, A.V., 2010. The specific slow afterhyperpolarization inhibitor UCL2077 is a subtype-selective blocker of the epilepsy associated KCNQ channels. Mol. Pharmacol. 78, 1088—1095. Available at: http://www.pubmedcentral.nih.gov/articlerender.fcgi?artid=2993466&tool=pmcentrez&rendertype=abstract. (Accessed 3 July 2015).

Song, W.J., Tkatch, T., Baranauskas, G., Ichinohe, N., Kitai, S.T., Surmeier, D.J., 1998. Somatodendritic depolarization-activated potassium currents in rat neostriatal cholinergic interneurons are predominantly of the A type and attributable to coexpression of Kv4.2 and Kv4.1 subunits. J. Neurosci. 18, 3124—3137. Available at: http://www.ncbi.nlm.nih.gov/pubmed/9547221. (Accessed 31 March 2015).

Sun, W., Yang, F., Wang, Y., Fu, H., Yang, Y., Li, C.-L., Wang, X.-L., Lin, Q., Chen, J., 2017. Contribution of large-sized primary sensory neuronal sensitization to mechanical allodynia by upregulation of hyperpolarization-activated cyclic nucleotide gated channels via cyclooxygenase 1 cascade. Neuropharmacology 113, 217—230. Available at: http://www.ncbi.nlm.nih.gov/pubmed/27743933. (Accessed 15 January 2018).

Tatulian, L., Delmas, P., Abogadie, F.C., Brown, D.A., 2001. Activation of expressed KCNQ potassium currents and native neuronal M-type potassium currents by the anti-convulsant drug retigabine. J. Neurosci. 21, 5535—5545. Available at: http://www.ncbi.nlm.nih.gov/pubmed/11466425. (Accessed 8 January 2018).

Tubert, C., Taravini, I.R.E., Flores-Barrera, E., Sánchez, G.M., Prost, M.A., Avale, M.E., Tseng, K.Y., Rela, L., Murer, M.G., 2016. Decrease of a current mediated by Kv1.3 channels causes striatal cholinergic interneuron hyperexcitability in experimental parkinsonism. Cell Rep. 16, 2749—2762. Available at: http://linkinghub.elsevier.com/retrieve/pii/S2211124716310622. (Accessed 2 January 2018).

Tzingounis, A.V., Heidenreich, M., Kharkovets, T., Spitzmaul, G., Jensen, H.S., Nicoll, R.A., Jentsch, T.J., 2010. The KCNQ5 potassium channel mediates a component of the afterhyperpolarization current in mouse hippocampus. Proc. Natl. Acad. Sci. U. S. A. 107, 10232—10237. Available at: http://www.pnas.org/cgi/doi/10.1073/pnas.1004644107. (Accessed 19 January 2018).

Villalonga, N., David, M., Bielańska, J., González, T., Parra, D., Soler, C., Comes, N., Valenzuela, C., Felipe, A., 2010. Immunomodulatory effects of diclofenac in leukocytes through the targeting of Kv1.3 voltage-dependent potassium channels. Biochem. Pharmacol. 80, 858—866. Available at: http://linkinghub.elsevier.com/retrieve/pii/S0006295210003515. (Accessed 12 January 2018).

Voilley, N., de Weille, J., Mamet, J., Lazdunski, M., 2001. Nonsteroid anti-inflammatory drugs inhibit both the activity and the inflammation-induced expression of acid-sensing ion channels in nociceptors. J. Neurosci. 21, 8026—8033. Available at: http://www.ncbi.nlm.nih.gov/pubmed/11588175. (Accessed 12 January 2018).

Wang, H.S., Pan, Z., Shi, W., Brown, B.S., Wymore, R.S., Cohen, I.S., Dixon, J.E., McKinnon, D., 1998. KCNQ2 and KCNQ3 potassium channel subunits: molecular correlates of the M-channel. Science 282, 1890—1893. Available at: http://www.ncbi.nlm.nih.gov/pubmed/9836639. (Accessed 8 January 2018).

Watanabe, K., Kimura, M., 1998. Dopamine receptor-mediated mechanisms involved in the expression of learned activity of primate striatal neurons. J. Neurophysiol. 79, 2568—2580. Available at: http://www.ncbi.nlm.nih.gov/pubmed/9582229. (Accessed 8 July 2015).

Wickenden, A.D., Yu, W., Zou, A., Jegla, T., Wagoner, P.K., 2000. Retigabine, a novel anti-convulsant, enhances activation of KCNQ2/Q3 potassium channels. Mol. Pharmacol. 58, 591—600. Available at: http://www.ncbi.nlm.nih.gov/pubmed/10953053. (Accessed 8 January 2018).

Wickenden, A.D., Zou, A., Wagoner, P.K., Jegla, T., 2001. Characterization of KCNQ5/Q3 potassium channels expressed in mammalian cells. Br. J. Pharmacol. 132, 381—384. Available at: http://www.ncbi.nlm.nih.gov/pubmed/11159685. (Accessed 10 January 2018).

Wilson, C.J., 2005. The mechanism of intrinsic amplification of hyperpolarizations and spontaneous bursting in striatal cholinergic interneurons. Neuron 45, 575—585. Available at: http://www.ncbi.nlm.nih.gov/pubmed/15721243. (Accessed 21 April 2015).

Witten, I.B., Lin, S.-C., Brodsky, M., Prakash, R., Diester, I., Anikeeva, P., Gradinaru, V., Ramakrishnan, C., Deisseroth, K., 2010. Cholinergic interneurons control local circuit activity and cocaine conditioning. Science 330, 1677—1681. Available at: http://www.ncbi.nlm.nih.gov/pubmed/21164015. (Accessed 2 January 2018).

Won, L., Ding, Y., Singh, P., Kang, U.J., 2014. Striatal cholinergic cell ablation attenuates L-DOPA induced dyskinesia in Parkinsonian mice. J. Neurosci. 34, 3090—3094. Available at: http://www.pubmedcentral.nih.gov/articlerender.fcgi?artid=3931510&tool=pmcentrez&rendertype=abstract. (Accessed 22 June 2015).

Wu, W.W., Chan, C.S., Surmeier, D.J., Disterhoft, J.F., 2008. Coupling of l-type Ca^{2+} Channels to K$_V$7/KCNQ channels creates a novel, activity-dependent, homeostatic intrinsic plasticity. J. Neurophysiol. 100, 1897—1908. Available at: http://www.ncbi.nlm.nih.gov/pubmed/18715900. (Accessed 2 January 2018).

Yue, C., Yaari, Y., 2006. Axo-somatic and apical dendritic kv7/m channels differentially regulate the intrinsic excitability of adult rat CA1 pyramidal cells. J. Neurophysiol. 95, 3480—3495. Available at: http://www.ncbi.nlm.nih.gov/pubmed/16495357. (Accessed 2 January 2018).

Zhang, Y.-F., Cragg, S.J., 2017. Pauses in striatal cholinergic interneurons: what is revealed by their common themes and variations? Front. Syst. Neurosci. 11, 80. Available at: http://www.ncbi.nlm.nih.gov/pubmed/29163075. (Accessed 23 January 2018).